Transient Multipole Expansion for Heat Transfer in Ground Heat Exchangers

Carlos Prieto [a] and Massimo Cimmino[a]

[a]Department of Mechanical Engineering, Polytechnique Montréal, Case Postale 6079, Succursale "Centre-ville," Montréal, Québec, H3C 3A7, Canada

ARTICLE HISTORY
Compiled December 3, 2020

ABSTRACT
A transient multipole method for short-term simulations of ground heat exchangers (GHEs) is presented. The two-dimensional unsteady heat equation over a GHE cross-section is separated into two problems: (i) a transient heat equation with homogeneous boundary conditions, and (ii) a steady-state heat equation with non-homogeneous boundary conditions. An eigenfunction expansion is proposed for the solution of the transient heat equation, where the treatment of boundary conditions is considered by a multipole expansion of the eigenfunctions. A singular value decomposition is applied to extract the eigenvalues of the problem. The solution of the steady-state heat equation is obtained from a multipole expansion. The proposed method is validated against reference results for the evaluation of the eigenvalues and for the steady-state temperature field. The complete transient solution is validated against finite element analysis simulations. The proposed method is meshless, and its accuracy is only dependent on the evaluation of eigenvalues and on the number of terms in each of the multipole expansions.

1. Introduction

Ground-coupled heat pump (GCHP) systems consist in one or multiple heat pumps that supply heating and cooling to a building by extracting or rejecting heat to one or multiple boreholes, i.e. the bore field or ground heat exchanger (GHE). A GHE is composed of a drilled hole into which one or several U-tubes are inserted (or alternatively, coaxial pipes) to circulate the heat carrier fluid, and then backfilled with grouting material. The design of GCHP systems aims at evaluating the required GHE length to maintain the temperature of the secondary fluid circulating in the GHE within an acceptable range to ensure safe and efficient operation of the system. The fluid and ground temperatures evolve during the operation of the system following the extraction and rejection of heat to the ground through the GHE. The short-term response of the GHE at time-scales of minutes to a few hours, corresponding to the time-scales of on/off and daily operation of the system, has been shown to have a significant impact on the required GHE length and on the energy use of the GCHP (Bernier & Shirazi, 2013). The short-term response of the GHE is driven by the transit of the fluid through the U-tube and the thermal capacity of borehole materials (i.e. the fluid, pipe and grout), and thus their inclusion into simulation models is required

CONTACT Carlos Prieto. Email: carlos.prieto@polymtl.ca

for accurate temperature predictions at short time-scales.

The classical approach to the heat transfer modelling of the interior of a borehole is through the thermal resistance analogy, where thermal interaction between pairs of pipes and between individual pipes and the ground are represented by a network of thermal resistances. The multipole method, introduced by Bennet et al. (1987) and further developed by Claesson & Bennet (1987) and Claesson & Hellström (2011), provides an analytical solution to the two-dimensional steady-state heat conduction in a borehole cross-section and enables the evaluation of the thermal resistances of a borehole. The multipole method consists in the construction of the exact solution to the heat equation by superimposing solutions translated at each pole (i.e. at each pipe) to apply the boundary conditions of the heat transfer problem. While analytical steady-state methods, such as the multipole method, provide exact solutions to the heat transfer inside the borehole, they are not able to accurately simulate the short-term response of the borehole, before quasi-steady-state conditions (or constant heat-flux conditions) are attained within the borehole.

Authors have proposed solutions to the transient heat transfer in a GHE by introducing the equivalent pipe assumption, which consists in representing all pipes by a single equivalent pipe with appropriately chosen dimensions and thermal properties to create a one-dimensional geometry with similar thermal characteristics to the real two-dimensional geometry. The simplified one-dimensional geometry has facilitated the development of analytical and numerical solutions to the transient heat transfer of GHEs. Bose et al. (1985) applied a conformal mapping technique to obtain an equivalent pipe model of a borehole. The method was used by Gu & O'Neal (1998) to solve the steady-state heat conduction equation and calculate fluid temperatures under the assumption of constant thermal conductivity coefficients. Shonder & Beck (1999) applied a finite difference scheme to solve the transient heat transfer in the equivalent geometry. The authors used their numerical model to analyze field monitored data and estimate the thermal properties of the GHE and the soil using a parameter estimation technique. Young (2004) adapted the Buried Electrical Cable solution of Carslaw & Jaeger (1959) to the simulation of boreholes, with the thermal capacitances of the grout and the fluid inside the equivalent pipes allocated to the sheat and core regions of the buried electric cable, respectively. Lamarche & Beauchamp (2007) developed an analytical solution to the transient heat transfer in the equivalent geometry with an imposed heat flux at the equivalent pipe. Bandyopadhyay et al. (2008) proposed an analytical solution in the Laplace domain where the thermal capacity of the fluid is introduced as a virtual solid with a lumped capacitance. In their work, Laplace domain solutions were obtained for the equivalent pipe GHE. A time domain solution is then obtained by means of the Gaver–Stehfest algorithm for inversion of the Laplace domain solution (Stehfest, 1970). Time-domain solutions were later proposed by Javed & Claesson (2011) and by Lamarche (2015). The dimensions and thermal characteristics of the single equivalent pipe geometry are chosen to preserve the total thermal resistance and the total lumped capacitance of the GHE. The short-term response of the GHE is thus only approximated due to the centrally located pipe which does not present the same distribution of heat transfer than multiple off-centered pipes.

Transient heat transfer in geothermal boreholes with a simplified equivalent pipe geometry was also solved numerically. Xu & Spitler (2006) developed a finite volume model of a GHE, where the thermal capacity of the fluid is included in an annular region within the pipe in the equivalent geometry. Brussieux & Bernier (2019) presented a hybrid variant of this approach, modelling the ground as a semi-infinite media using the Cylindrical Heat Source (CHS) solution of Carslaw & Jaeger (1959). The authors

introduced dimensionless parameters to define universal short time-step g^*-functions which take into account the short-time behavior of GHEs. Short time-step g-functions were introduced by Yavuzturk (1999) who proposed a two-dimensional finite volume method in cylindrical coordinates to evaluate the thermal response of GHEs, taking into account the effects of the thermal capacities of the grout and pipe materials. Short time-step g-functions (and g^*-functions) provide an extension of Eskilson's g-functions (Eskilson, 1987) to short time-step simulations and enable the design of GHEs with attention to short-time effects.

Li & Lai (2013) proposed to model the short-term response of a GHE using the infinite composite-medium line source (ICMLS) analytical solution, in which each pipe is represented as a line source in the grout of the GHE. The model accounts for the split of heat transfer rate between the pipes, since each pipe is modelled and may have different external wall temperatures. The model was validated by Yang & Li (2014) using a finite volume method (FVM). The limitation of this method is that the pipes are simplified as lines (rather than cylinders), and thus the distribution of temperatures and heat transfer rate on the perimeter of the pipes is not taken into account.

Another class of simulation models aimed at the simulation of the short-time response of GHEs is composed of so-called thermal resistance and capacitance (TRC) models. Rather than attempting to solve the transient heat equation, this class of models introduces thermal capacitance nodes to the network of thermal resistances inferred from the multipole method or its approximations. Zarella et al. (2011) extended the capacity resistance model (CaRM) of De Carli et al. (2010) to introduce thermal capacity nodes at the core and at the sheat of the borehole. Bauer et al. (2011a,b) developed a TRC model where thermal capacity nodes are introduced to represent the thermal capacity of half the GHE (for a single U-tube borehole). Pasquier & Marcotte (2012) proposed an extension of the TRC model where each of the fluid, pipe and grout are represented as a series of thermal resistances and capacitances. The distribution of fluid temperatures along the GHE can then be obtained by coupling a series of TRC models each representing a segment of the GHE (Pasquier & Marcotte, 2014). Minaei & Maerefat (2017) observed that negative values of thermal resistances can be obtained in TRC models. While negative values have no effect on the accuracy of steady-state temperatures, they can cause a non-physical thermal response at short-time scales. The authors proposed a modified thermal resistance network to eliminate the negative thermal resistances. Like equivalent pipe geometries, TRC models preserve the total thermal resistance and the total lumped capacitance of the GHE. Thermal capacitances are split into core and exterior zones of the GHE, and thus the short-term response is expected to be more accurate but is still an estimate of the exact short-term response. The distribution of thermal capacitance nodes are based on arbitrary geometrical divisions of the GHE cross-sectional area and none of the surveyed methods are applicable to non-symmetric pipe configurations.

As per the surveyed literature, current analytical methods to solve the transient heat conduction equation in a cross-section of a GHE are limited to simplified one-dimensional geometries in cylindrical coordinates. The short-term response of the real geometry requires the solution of a partial differential equation (i.e. the heat equation) in a multiply-connected two-dimensional domain (i.e. a domain with multiple boundaries). Solutions to this type of problem have been obtained in other fields of application of heat transfer analysis. Commonly applied techniques are finite integral transforms (often applied to single layer materials), Green functions, orthogonal expansions, and Laplace transforms (Carslaw & Jaeger, 1959). In Cartesian coordi-

nates, examples of applications of these techniques are Salt (1983) and Mikhailov & Özisik (1986) (orthogonal expansion technique in slabs) as well as Haji-Sheikh & Beck (2002) (Green function). In cylindrical coordinates, example works are Abdul Azeez & Vakakis (2000) (integral transform) and Milošević & Raynaud (2004) (orthogonal expansion in cylinders).

Numerical methods, such as finite difference, finite volume, finite element and boundary element methods, are often used to solve partial differential equations in multiple dimensions. The accuracy of these methods strongly depends on the quality of the mesh, and the generation of the mesh is complicated in cases where the geometry of the problem is highly variable —for instance, the number and position of pipes in a GHE. These methods also become time-intensive when applied to higher dimensions. There has been a growing interest in meshless methods over the past decade for heat transfer applications (Nguyen et al., 2008). A popular class of meshless methods are Trefftz methods (Trefftz, 1926), which consist in approximating a regular solution to a partial differential equation problem in variational form. This technique is extended to use analytical solutions of the governing equations (e.g. Fourier-Bessel series) (Kita & Kamiya, 1995). These methods are meshless. They can thus be implemented without the complexity of domain meshing and only require matching the boundaries over specific portions in a domain.

This paper presents a new method to solve the transient heat conduction problem in $\mathbb{R}^2$ for a circular multiply-connected domain representing a cross-section of a GHE with multiple pipes. The separation of variables is applied to separate the problem into two equations, a Helmholtz partial differential equation for space and an ordinary differential equation for time. The complete solution is obtained by the superposition of a solution of the steady-state problem with inhomogeneous boundary conditions and a solution of a transient problem with homogeneous boundary conditions (i.e. a Sturm-Liouville problem). The transient problem is solved by applying a multipole expansion technique (Wu & Kishk, 2008; Záviška, 1913), using an eigenfunction expansion of the solution. The solution considers constant fluid temperatures within each pipe. A scheme to update the coefficients of the multipole expansion is proposed to consider time-dependent fluid temperatures. The proposed method is validated by comparison with the results of Chen et al. (2001, 2004) for the evaluation of the eigenvalues of the expansion, with the results of Claesson & Hellström (2011) for the solution of the steady-state problem, and to finite element analysis (FEA) simulations for the complete transient solution.

2. Mathematical Model

A mathematical model for 2D transient heat conduction in geothermal boreholes is presented. The model assumes homogeneous, isotropic and constant physical properties for the grout and the ground, with uniform temperature at time $t = 0$. The thermal capacity of the fluid flowing through the pipes and that of the pipe material are neglected. Axial heat transfer, through advection of the fluid flowing through the pipes and conduction in the vertical direction, is neglected and thus only pure conduction on the horizontal plane in the grout and ground is considered. The fluid to outer pipe wall thermal resistances, combining the film thermal resistances and the conduction thermal resistance through the pipe walls, is constant for each pipe.

Figure 1 shows the horizontal cross-section of a geothermal borehole with $N = 2$ pipes (i.e. a single U-tube) as well as the computational domain of the mathematical

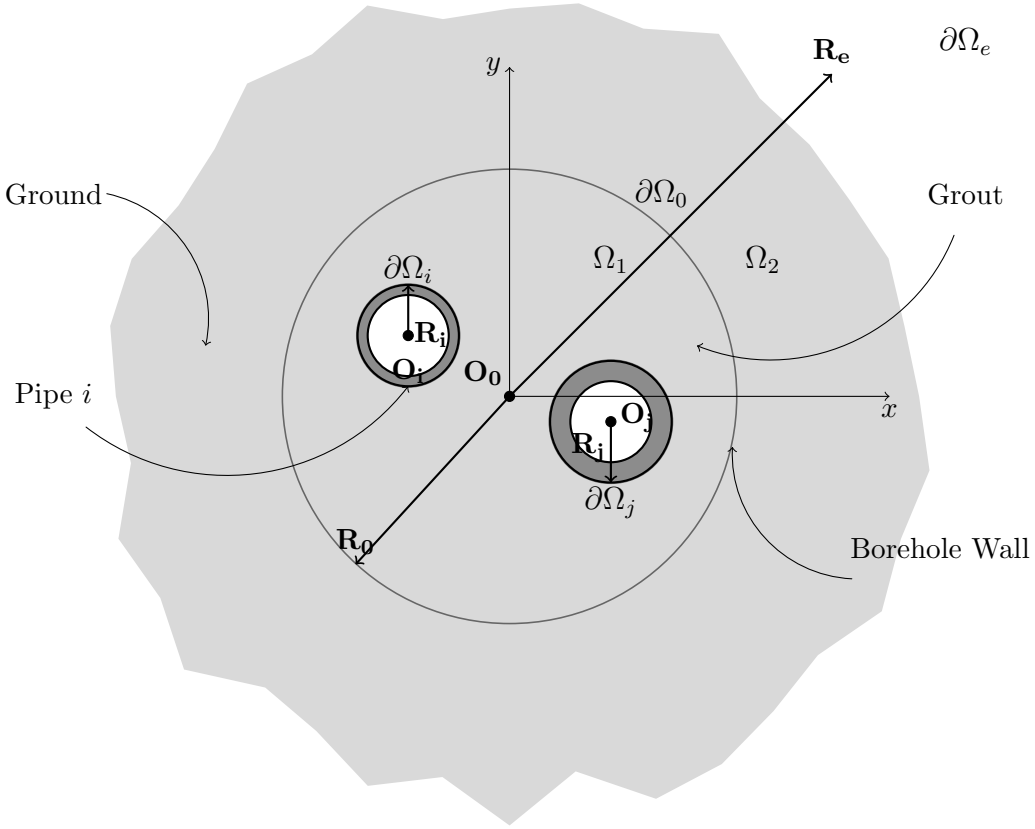

Figure 1. Ground heat exchanger domain geometry

model. The borehole, centered at O_0, has a radius R_0 and each pipe i, centered at O_i, has an external radius R_i. The computational domain $\Omega(=\Omega_1 \cup \Omega_2)$ comprises the grout sub-domain Ω_1 and the ground sub-domain Ω_2, with $\partial\Omega_0$ the interface between the grout and the ground (i.e. the borehole wall). The interior boundaries $\partial\Omega_i$ correspond with the external wall of each pipe i. The domain extends to a radial distance R_e from the borehole center, corresponding with the external boundary $\partial\Omega_e$. R_e is considered infinite, and thus the ground domain Ω_2 is unbounded. A point $\mathbf{x} = (\rho, \phi)$ in cylindrical coordinates could be centered at any pole O_k, with $\mathbf{x}_k = (\rho_k, \phi_k)$, as shown on Figure 2. Throughout the paper, the non-index coordinates $\mathbf{x} = (\rho, \phi)$ are used when it is not needed to express the coordinates at any particular pole.

The governing equation for heat transfer for calculating the temperature $T_i = T_i(\mathbf{x}, t)$ is given by the transient heat conduction equation:

$$\frac{1}{\alpha_i}\frac{\partial T_i}{\partial t} = \nabla^2 T_i \text{ in } \Omega_i,\ i = 1, 2 \tag{1}$$

where T_1 is the temperature in the grout domain Ω_1, T_2 is the temperature in the ground domain Ω_2, and α_i is the thermal diffusivity at each domain Ω_i.

The fluid temperature T_{f_k} at each pipe k is prescribed. As such, the boundary condition at the external wall of each pipe is:

$$-\beta_k R_k \left.\frac{\partial T_1}{\partial \rho_k}\right|_{R_k} + T_1 = T_{f_k} \text{ on } \partial\Omega_k,\ k = 1, \ldots, N \tag{2}$$

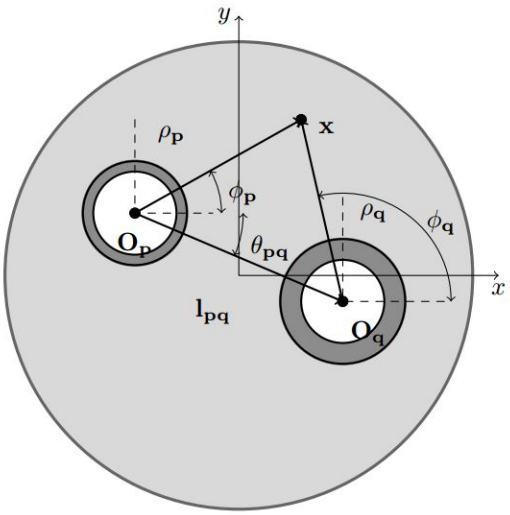

Figure 2. Translation of coordinates

where $\beta_k = 2\pi k_b E_k$ is the dimensionless fluid to outer pipe wall thermal resistance of pipe k; with k_b the grout thermal conductivity and E_k the fluid to outer pipe wall thermal resistance of pipe k.

Continuity is imposed at the borehole wall ($\partial\Omega_0$):

$$-k_b \left.\frac{\partial T_1}{\partial \rho_0}\right|_{R_0} = -k_s \left.\frac{\partial T_2}{\partial \rho_0}\right|_{R_0} \text{ on } \partial\Omega_0 \tag{3}$$

and

$$T_1|_{R_0} = T_2|_{R_0} \text{ on } \partial\Omega_0 \tag{4}$$

where k_s is the thermal conductivity of the ground.

The temperature at the exterior domain boundary $\partial\Omega_e$ (at $R_e \to \infty$) is equal to the undisturbed ground temperature:

$$T_2(R_e, \phi, t)|_{R_e \to \infty} = T^0 \text{ on } \partial\Omega_e \tag{5}$$

At time $t = 0$, the initial grout and ground temperature are uniform and equal to the undisturbed ground temperature:

$$T_i(\rho, \phi, 0) = T^0 \text{ in } \Omega_i,\ i = 1, 2 \tag{6}$$

The set of boundary conditions (Eqs. 2-6) is non-homogeneous. To obtain a solution to the temperature, the problem (Eq. 1) is separated into a transient problem with homogeneous boundary conditions (i.e. a Sturm-Liouville problem) and a steady-state problem with non-homogeneous boundary conditions. The complete solution becomes $T_i = T_{i_h} + T_{i_{ss}}$, where $T_{i_h} = T_{i_h}(\rho, \phi, t)$ is the solution to the homogeneous transient boundary conditions and $T_{i_{ss}} = T_{i_{ss}}(\rho, \phi)$ is the steady state solution of Eq. 1.

The governing equation as well as boundary and initial conditions of the transient

problem with homogeneous boundary conditions are given by:

$$\frac{1}{\alpha_i}\frac{\partial T_{i_h}}{\partial t} = \nabla^2 T_{i_h} \text{ in } \Omega_i,\ i = 1, 2 \tag{7a}$$

$$-\beta_k R_k \frac{\partial T_{1_h}}{\partial \rho_k}\bigg|_{R_k} + T_{1_h} = 0 \text{ on } \partial\Omega_k,\ k = 1, \ldots, N \tag{7b}$$

$$-k_b \frac{\partial T_{1_h}}{\partial \rho_0}\bigg|_{R_0} = -k_s \frac{\partial T_{2_h}}{\partial \rho_0}\bigg|_{R_0} \text{ on } \partial\Omega_0 \tag{7c}$$

$$T_{1_h}|_{R_0} = T_{2_h}|_{R_0} \text{ on } \partial\Omega_0 \tag{7d}$$

$$T_{2_h}(R_e, \phi, t)|_{R_e\to\infty} = 0 \text{ on } \partial\Omega_e \tag{7e}$$

$$T_{i_h}(\rho, \phi, 0) = T^0 - T_{i_{ss}} \text{ in } \Omega_i,\ i = 1, 2 \tag{7f}$$

The governing equation as well as boundary and initial conditions of the steady-state problem with non-homogeneous boundary conditions are given by:

$$\nabla^2 T_{i_{ss}} = 0 \text{ in } \Omega_i,\ i = 1, 2 \tag{8a}$$

$$-\beta_k R_k \frac{\partial T_{1_{ss}}}{\partial \rho_k}\bigg|_{R_k} + T_{1_{ss}} = T_{f_k} \text{ on } \partial\Omega_k,\ k = 1, \ldots, N \tag{8b}$$

$$-k_b \frac{\partial T_{1_{ss}}}{\partial \rho_0}\bigg|_{R_0} = -k_s \frac{\partial T_{2_{ss}}}{\partial \rho_0}\bigg|_{R_0} \text{ on } \partial\Omega_0 \tag{8c}$$

$$T_{1_{ss}}|_{R_0} = T_{2_{ss}}|_{R_0} \text{ on } \partial\Omega_0 \tag{8d}$$

$$T_{2_{ss}}(R_e, \phi)|_{R_e\to\infty} = T^0 \text{ on } \partial\Omega_e \tag{8e}$$

The solutions to both problems are presented in the next sections. Note that even though the solution to the transient problem (Eq. 7) is presented first, its initial condition (Eq. 7f) is dependent upon the solution to the steady state problem (Eq. 8).

2.1. Transient Heat Equation with Homogeneous Boundary Conditions

The transient problem with homogeneous boundary conditions (Eq. 7) is solved by means of spatial-time decomposition using separation of variables. Assuming the solution is $T_{i_h} = X_i(\rho, \phi)\tau_i(t)$, then the problem becomes:

$$\frac{\nabla^2 X_i}{X_i} = \frac{\dot{\tau}_i}{\alpha_i \tau_i} = -\lambda_i^2 \tag{9}$$

where λ is the eigenvalue associated with the homogeneous boundary problem partial differential equation (PDE). Note that $\lambda > 0$ and that λ is not unique (Abdul Azeez & Vakakis, 2000; Mikhailov & Özisik, 1986).

The solution for τ_i is straightforward:

$$\tau_i(t) = e^{-\lambda_i^2 \alpha_i t} \tag{10}$$

The problem for X_i defined in Eq. 9 takes the form of the Helmholtz equation. The Helmholtz equation is encountered in many fields, for example in the study of wave propagation in continuous media (Linton & Evans, 1990), scattering with non-

obstacles (Martin, 2006), or electrical propagation in integrated circuits (Wu & Kishk, 2008). The complete Helmholtz homogeneous boundary problem is well defined and has a unique solution.

The governing equation as well as boundary conditions for X_i are given by:

$$\nabla^2 X_i + \lambda_i^2 X_i = 0 \text{ in } \Omega_i,\ i = 1, 2 \tag{11a}$$

$$-\beta_k R_k \frac{\partial X_1}{\partial \rho_k}\bigg|_{R_k} + X_1 = 0 \text{ on } \partial\Omega_k,\ k = 1, \ldots, N \tag{11b}$$

$$-k_b \frac{\partial X_1}{\partial \rho_0}\bigg|_{R_0} = -k_s \frac{\partial X_2}{\partial \rho_0}\bigg|_{R_0} \text{ on } \partial\Omega_0 \tag{11c}$$

$$X_1|_{R_0} = X_2|_{R_0} \text{ on } \partial\Omega_0 \tag{11d}$$

$$X_2(R_e, \phi)|_{R_e \to \infty} = 0 \text{ on } \partial\Omega_e \tag{11e}$$

The continuity condition (Eqs. 11c-11d) results in the eigenvalue connection between the grout and ground domains (Ω_1 and Ω_2), with $\lambda_2 = \lambda_1\sqrt{\alpha_1/\alpha_2}$ (Salt, 1983; Tittle, 1965). Eq. 11 was solved to obtain its solution at any point $\mathbf{x} = (\rho, \phi)$ in Ω by Chen et al. (2005, 2010) in the context of acoustic analysis of multiply-connected membranes. Here, the solution is presented for transient homogeneous heat transfer with mixed boundary conditions.

A complete eigenfunction expansion for the solution in a circular multiply-connected domain Ω is proposed as follows:

$$X_i(\rho, \phi) = \sum_{m=-M}^{M} \gamma_m \psi(\rho, \phi) \tag{12}$$

where $\psi(\mathbf{x})$ is the Trefftz basis at pole O and γ_m are the coefficient matching the boundaries. The number of terms in the expansion is formally infinite, but is reduced to $2M + 1$ to obtain a finite sum.

For the circular multiply-connected domain Ω, the following Trefftz basis for a point $\mathbf{x}_p = (\rho_p, \phi_p)$ related to a pole O_p, is defined for a circular boundary $\partial\Omega_p$ with radius R_p (Figure 2):

$$\psi(\rho_p, \phi_p) = \begin{cases} J_m(\lambda\rho_p)e^{im\phi_p} & \text{if } \rho_p < R_p \\ H_m^{(1)}(\lambda\rho_p)e^{im\phi_p} & \text{if } \rho_p > R_p \end{cases} \tag{13}$$

where J and $H^{(1)}$ are the Bessel and Hankel functions of the first kind, respectively.

To obtain the solution of Eq. 11 for any N number of pipes, ψ needs to be expressed at any pole O_j in the domain Ω_1. For the translation of coordinates shown in Figure 2, the Graf-Gegenbauer addition theorem (Graf, 1893) yields:

$$J_m(\lambda\rho_p)e^{im\phi_p} = \sum_{n=-\infty}^{\infty} J_{m-n}(\lambda l_{pq})e^{i(m-n)\theta_{pq}} J_n(\lambda\rho_q)e^{in\phi_q} \tag{14a}$$

$$H_m^{(1)}(\lambda\rho_p)e^{im\phi_p} = \begin{cases} \sum_{n=-\infty}^{\infty} J_{m-n}(\lambda l_{pq})e^{i(m-n)\theta_{pq}} H_n^{(1)}(\lambda\rho_q)e^{in\phi_q} & \text{if } l_{pq} < \rho_q \\ \sum_{n=-\infty}^{\infty} H_{m-n}^{(1)}(\lambda l_{pq})e^{i(m-n)\theta_{pq}} J_n(\lambda\rho_q)e^{in\phi_q} & \text{if } l_{pq} > \rho_q \end{cases} \tag{14b}$$

Superimposing the contributions of all poles (O_j) and considering only $2M+1$ terms in Eq. 14, Eq. 13 in Ω_1 becomes:

$$X_1(\mathbf{x}) = \sum_{m=-M}^{M} \gamma_m^0 J_m(\lambda_1 \rho_0) e^{im\phi_0} + \sum_{j=1}^{N} \sum_{m=-M}^{M} \gamma_m^j H_m^{(1)}(\lambda_1 \rho_j) e^{im\phi_j} \tag{15}$$

The solution in Ω_2 follows the same procedure but with only 1 internal pipe at $\partial\Omega_0$:

$$X_2(\mathbf{x}) = \sum_{m=-M}^{M} \delta_m^0 H_m^{(1)}(\lambda_2 \rho_0) e^{im\phi_0} \tag{16}$$

As Ω_2 is unbounded, Eq. 16 vanishes if $R_e \to \infty$, as shown by the asymptotic expansion expressed in Abramowitz & Stegun (1972). Eq. 11e is thus satisfied. Therefore, the Trefftz basis for Ω_2 defined in Eq. 13 is considered exterior domain and thus only the Hankel function is required.

The boundary conditions in Eq. 11 require the evaluation of X_1 and X_2 and their derivatives at all boundaries ($\partial\Omega_j$) in Ω_1 and Ω_2, respectively. At the borehole wall ($\partial\Omega_0$):

$$\begin{aligned} X_1(R_0, \phi_0) = & \sum_{m=-M}^{M} \gamma_m^0 J_m(\lambda_1 R_0) e^{im\phi_0} \\ & + \sum_{j=1}^{N} \sum_{m=-M}^{M} \gamma_m^j \sum_{n=-M}^{M} J_{m-n}(\lambda_1 l_{j0}) e^{i(m-n)\theta_{j0}} H_n^{(1)}(\lambda_1 R_0) e^{in\phi_0} \end{aligned} \tag{17a}$$

$$X_2(R_0, \phi_0) = \sum_{m=-M}^{M} \delta_m^0 H_m^{(1)}(\lambda_2 R_0) e^{im\phi_0} \tag{17b}$$

$$\begin{aligned} \left.\frac{\partial X_1}{\partial \rho_0}\right|_{R_0} = & \lambda_1 \sum_{m=-M}^{M} \gamma_m^0 J'_m(\lambda_1 R_0) e^{im\phi_0} \\ & + \lambda_1 \sum_{j=1}^{N} \sum_{m=-M}^{M} \gamma_m^j \sum_{n=-M}^{M} J_{m-n}(\lambda_1 l_{j0}) e^{i(m-n)\theta_{j0}} H'^{(1)}_n(\lambda_1\ R_0) e^{in\phi_0} \end{aligned} \tag{17c}$$

$$\left.\frac{\partial X_2}{\partial \rho_0}\right|_{R_0} = \lambda_2 \sum_{m=-M}^{M} \delta_m^0 H'^{(1)}_m(\lambda_2 R_0) e^{im\phi_0} \tag{17d}$$

At the external wall of each pipe ($\partial\Omega_l$):

$$\begin{aligned} X_1(R_l,\phi_l) = &\sum_{m=-M}^{M}\gamma_m^0\sum_{n=-M}^{M}J_{m-n}(\lambda_1 l_{0l})e^{i(m-n)\theta_{0l}}J_n(\lambda_1 R_l)e^{in\phi_l} \\ &+\sum_{m=-M}^{M}\gamma_m^l H_m^{(1)}(\lambda_1 R_l)e^{im\phi_l} \\ &+\sum_{j=1,j\neq l}^{N}\sum_{m=-M}^{M}\gamma_m^j\sum_{n=-M}^{M}g_{mn} \end{aligned} \tag{18a}$$

$$\begin{aligned} \left.\frac{\partial X_1}{\partial\rho_l}\right|_{R_l} = &\lambda_1\sum_{m=-M}^{M}\gamma_m^0\sum_{n=-M}^{M}J_{m-n}(\lambda_1 l_{0l})e^{i(m-n)\theta_{0l}}J_n'(\lambda_1 R_l)e^{in\phi_l} \\ &+\lambda_1\sum_{m=-M}^{M}\gamma_m^l H_m'^{(1)}(\lambda_1 R_l)e^{im\phi_l} \\ &+\lambda_1\sum_{j=1,j\neq l}^{N}\sum_{m=-M}^{M}\gamma_m^j\sum_{n=-M}^{M}g'_{mn} \end{aligned} \tag{18b}$$

where

$$g_{mn} = \begin{cases} J_{m-n}(\lambda_1 l_{jl})e^{i(m-n)\theta_{jl}}H_n^{(1)}(\lambda_1 R_l)e^{in\phi_l} & \text{if } l_{jl} < R_l \\ H_{m-n}^{(1)}(\lambda_1 l_{jl})e^{i(m-n)\theta_{jl}}J_n(\lambda_1 R_l)e^{in\phi_l} & \text{if } l_{jl} > R_l \end{cases} \tag{19a}$$

$$g'_{mn} = \begin{cases} J_{m-n}(\lambda_1 l_{jl})e^{i(m-n)\theta_{jl}}H_n'^{(1)}(\lambda_1 R_l)e^{in\phi_l} & \text{if } l_{jl} < R_l \\ H_{m-n}^{(1)}(\lambda_1 l_{jl})e^{i(m-n)\theta_{jl}}J_n'(\lambda_1 R_l)e^{in\phi_l} & \text{if } l_{jl} > R_l \end{cases} \tag{19b}$$

The substitution of Eqs. 17-19 into 11 yields a linear system $\mathbf{\Phi}\gamma = \mathbf{0}$, where the square matrix $\mathbf{\Phi}$ is a function of λ. Singular Value Decomposition (SVD) is used in order to extract the value λ of the square matrix $\mathbf{\Phi}$ by collecting the minimum singular value of the decomposition and finding the drop of this singular value. The multiplicity of λ is obtained, seeking how many singular values are equal to the minimum. The dimension of the matrix is dim $\mathbf{\Phi} = [(2M+1)(N+2)\times(2M+1)(N+2)]$. The solution γ is obtained at each eigenvalue λ by multiplying the eigenvector associated and $\mathbf{\Phi}$.

Recalling Eq. 7, the homogeneous solution is then calculated as a Fourier-Bessel expansion:

$$T_{i_h}(\rho,\phi,t) = \sum_{j=1}^{\infty}C_j X_i(\rho,\phi;\lambda_i^j)e^{-(\lambda_i^j)^2\alpha_i t} \tag{20}$$

where X_i is a quasi-orthogonal eigenfunction (Tittle, 1965) and λ_i^j is the j-th eigenvalue for the expansion in Ω_i.

The calculation of coefficients C_j requires imposing the initial condition and applying orthogonal conditions:

$$C_j = \frac{\frac{k_b}{\alpha_1}\int_{\Omega_1}(T^0 - T_{1_{ss}})\bar{X}_1 d\Omega_1 + \frac{k_s}{\alpha_2}\int_{\Omega_2}(T^0 - T_{2_{ss}})\bar{X}_2 d\Omega_2}{\frac{k_b}{\alpha_1}\int_{\Omega_1}X_1\bar{X}_1 d\Omega_1 + \frac{k_s}{\alpha_2}\int_{\Omega_2}X_2\bar{X}_2 d\Omega_2} \tag{21}$$

where $\bar{X}_i$ is the conjugate of X_i. It is important to point out that γ, δ and C_j are complex-valued, and thus Eq. 20 implies that only the real part of the temperature is considered. However, as long as Eq. 7 has real-valued initial and boundary conditions, the solution will have real temperature values.

2.2. Steady-State Heat Equation with Nonhomogeneous Boundary Conditions

A T-complete basis is required to obtain the solution to Eq. 8. Such a basis was proposed by Liu (2008) for the Laplace equation in a doubly-connected domain. In the present case, for $N+1$ poles, the temperature in Ω_1 is given by:

$$\begin{aligned} T_{1_{ss}} =& \alpha_0 + \sum_{m=1}^{h} \left[\alpha_m \left(\frac{\rho_0}{R_{max}} \right)^m \cos(m\phi_0) + \beta_m \left(\frac{\rho_0}{R_{max}} \right)^m \sin(m\phi_0) \right] \\ &+ \sum_{j=1}^{N} \left\{ \gamma_0^j \ln \rho_j + \sum_{m=1}^{h} \left[\gamma_m^j \left(\frac{\rho_j}{R_{min}} \right)^{-m} \cos(m\phi_j) + \delta_m^j \left(\frac{\rho_j}{R_{min}} \right)^{-m} \sin(m\phi_j) \right] \right\} \end{aligned} \tag{22}$$

and the temperature in Ω_2 (with only one pole shared by $\partial\Omega_0$ and $\partial\Omega_e$) is given by:

$$\begin{aligned} T_{2_{ss}} =& \alpha_0' + \sum_{m=1}^{h} \left[\alpha_m' \left(\frac{\rho_0}{R_e} \right)^m \cos(m\phi_0) + \beta_m' \left(\frac{\rho_0}{R_e} \right)^m \sin(m\phi_0) \right] \\ &+ \gamma_0' \ln \rho_0 + \sum_{m=1}^{h} \left[\gamma_m' \left(\frac{\rho_0}{R_{\min}} \right)^{-m} \cos(m\phi_0) + \delta_m' \left(\frac{\rho_0}{R_{\min}} \right)^{-m} \sin(m\phi_0) \right] \end{aligned} \tag{23}$$

where $R_{\min} = \min_{i \in \{1,\ldots,N\}} R_i$ is the minimum external radius of the pipes, $R_{max} \geq R_0$ is an arbitrary radius and is set equal to R_0, and h is the number of terms in the complete expansion (Eqs. 22-23). Note that γ_m^j are different from the preceding expansion in Eq. 15.

By definition Eqs. 22-23 have infinite terms but it is reduced here to the h first terms of the expansion. To have a unique solution, the coefficients that match boundaries, $\alpha_0, \alpha_m, ..., \delta_m'$, have to be unique and finite. For $R_e \to \infty$, Eq. 23 results in arbitrary values for α_m', β_m', and they are thus considered equal to 0. Also, γ_0' has to be equal to 0 for $T_{2_{ss}}$ to remain finite. Therefore, the solution of this problem results in the coefficient $\alpha_0' = T_{2_{ss}}(R_e, \phi)|_{R_e \to \infty} = T^0$. The presented method for steady-state allows to successfully allocate the boundary conditions for the unbounded domain Ω_2 and thus compute the coefficients in the T-basis.

For the translation of coordinates shown in Figure 2, an addition theorem was proposed by Bird & Steele (1992) for the Laplace equation in a multiply-connected

domain:

$$\rho_p^m \cos(m\phi_p) = \sum_{n=0}^{m} \binom{m}{n} (-1)^n \rho_p^{m-n} l_{pq}^n \cos(m\theta_{pq} + n(\phi_q - \theta_{pq})) \tag{24a}$$

$$\rho_p^m \sin(m\phi_p) = \sum_{n=0}^{m} \binom{m}{n} (-1)^n \rho_p^{m-n} l_{pq}^n \sin(m\theta_{pq} + n(\phi_q - \theta_{pq})) \tag{24b}$$

$$\rho_p^{-m} \cos(m\phi_p) = \begin{cases} \sum_{k=-1}^{\infty} \binom{m+k}{k+1} \frac{\rho_q^{k+1}}{l_{pq}^{k+m+1}} \cos[(k+1)\phi_q - (k+m+1)\theta_{pq}] & \text{if } l_{pq} > \rho_q \\ \sum_{k=-1}^{\infty} (-1)^m \binom{m+k}{k+1} \frac{l_{pq}^{k+1}}{\rho_p^{k+m+1}} \cos[(k+1)\theta_{pq} - (k+m+1)\phi_q] & \text{if } l_{pq} < \rho_q \end{cases} \tag{24c}$$

$$\rho_p^{-m} \sin(m\phi_p) = \begin{cases} \sum_{k=-1}^{\infty} \binom{m+k}{k+1} \frac{\rho_q^{k+1}}{l_{pq}^{k+m+1}} \sin[(k+1)\phi_q - (k+m+1)\theta_{pq}] & \text{if } l_{pq} > \rho_q \\ \sum_{k=-1}^{\infty} (-1)^m \binom{m+k}{k+1} \frac{l_{pq}^{k+1}}{\rho_p^{k+m+1}} \sin[(k+1)\theta_{pq} - (k+m+1)\phi_q] & \text{if } l_{pq} < \rho_q \end{cases} \tag{24d}$$

$$\ln \rho_p = \begin{cases} \ln(l_{pq}) - \sum_{m=1}^{\infty} \left(\frac{1}{m}\right) \left(\frac{\rho_p}{l_{pq}}\right)^m \cos[m(\theta_{pq} - \phi_q)] & \text{if } l_{pq} > \rho_q \\ \ln(\rho_q) - \sum_{m=1}^{\infty} \left(\frac{1}{m}\right) \left(\frac{l_{pq}}{\rho_p}\right)^m \cos[m(\theta_{pq} - \phi_q)] & \text{if } l_{pq} < \rho_q \end{cases} \tag{24e}$$

The boundary conditions in Eq. 8 require the evaluation of $T_{1_{ss}}$ and $T_{2_{ss}}$ and their derivatives at all boundaries ($\partial\Omega_j$) in Ω_1 and Ω_2, respectively. At the borehole wall

$(\partial\Omega_0)$:

$$T_{1_{ss}} = \alpha_0 + \sum_{m=1}^{h}\left[\alpha_m\left(\frac{R_0}{R_{max}}\right)^m\cos(m\phi_0) + \beta_m\left(\frac{R_0}{R_{max}}\right)^m\sin(m\phi_0)\right]$$
$$+\sum_{j=1}^{N}\left\{\gamma_0^j\left(\ln R_0 - \sum_{m=1}^{\infty}\left(\frac{1}{m}\right)\left(\frac{l_{j0}}{R_0}\right)^m\cos[m(\theta_{j0}-\phi_0)]\right)\right.$$
$$+\sum_{m=1}^{h}\sum_{k=-1}^{h}\left[\gamma_m^j(-1)^m\binom{m+k}{k+1}R_{min}^m\frac{l_{j0}^{k+1}}{R_0^{k+m+1}}\cos[(k+1)\theta_{j0}-(k+m+1)\phi_0]\right.$$
$$\left.\left.+\ \delta_m^j(-1)^m\binom{m+k}{k+1}R_{min}^m\frac{l_{j0}^{k+1}}{R_0^{k+m+1}}\sin[(k+1)\theta_{j0}-(k+m+1)\phi_0]\right]\right\} \tag{25a}$$

$$T_{2_{ss}} = T^0 + \sum_{m=1}^{h}\left[\gamma'_m\left(\frac{R_0}{R_{\min}}\right)^{-m}\cos(m\phi_0) + \delta'_m\left(\frac{R_0}{R_{\min}}\right)^{-m}\sin(m\phi_0)\right] \tag{25b}$$

$$\left.\frac{\partial T_{1_{ss}}}{\partial\rho_0}\right|_{R_0} = \sum_{m=1}^{h} m\left[\alpha_m\left(\frac{1}{R_{max}}\right)^m R_0^{m-1}\cos(m\phi_0) + \beta_m\left(\frac{1}{R_{max}}\right)^m R_0^{m-1}\sin(m\phi_0)\right]$$
$$+\sum_{j=1}^{N}\left\{\gamma_0^j\left(\frac{1}{R_0} + \sum_{m=1}^{\infty}\left(\frac{1}{R_0}\right)^{m+1} l_{j0}^m\cos[m(\theta_{j0}-\phi_0)]\right)\right.$$
$$-\sum_{m=1}^{h}\sum_{k=-1}^{h}\left[\gamma_m^j(-1)^m(k+m+1)\binom{m+k}{k+1}R_{min}^m\frac{l_{j0}^{k+1}}{R_0^{k+m+2}}\cos[(k+1)\theta_{j0}-(k+m+1)\phi_0]\right.$$
$$\left.\left.+\ \delta_m^j(-1)^m(k+m+1)\binom{m+k}{k+1}R_{min}^m\frac{l_{j0}^{k+1}}{R_0^{k+m+2}}\sin[(k+1)\theta_{j0}-(k+m+1)\phi_0]\right]\right\} \tag{25c}$$

$$\left.\frac{\partial T_{2_{ss}}}{\partial\rho_0}\right|_{R_0} = -\sum_{m=1}^{h} m\left[\alpha'_m\left(\frac{1}{R_{\min}}\right)^{-m} R_0^{-m-1}\cos(m\phi_0) + \beta'_m\left(\frac{1}{R_{\min}}\right)^{-m} R_0^{-m-1}\sin(m\phi_0)\right] \tag{25d}$$

At the external wall of each pipe ($\partial\Omega_l$):

$$
\begin{aligned}
T_{1_{ss}} = \alpha_0 &+ \sum_{m=1}^{h} \frac{1}{{R_{max}}^m} \left[\alpha_m \sum_{k=0}^{m} \binom{m}{k} (-1)^k R_l^{m-k} l_{0l}^k \cos[m\theta_{0l} + k(\phi_l - \theta_{0l})] \right. \\
&\left. + \beta_m \sum_{k=0}^{m} \binom{m}{k} (-1)^k R_l^{m-k} l_{0l}^k \sin[m\theta_{0l} + k(\phi_l - \theta_{0l})] \right] \\
&+ \gamma_0^l \ln R_l + \sum_{m=1}^{h} \left[\gamma_m^l \left(\frac{R_l}{R_{\min}} \right)^{-m} \cos(m\phi_l) + \delta_m^l \left(\frac{R_l}{R_{\min}} \right)^{-m} \sin(m\phi_l) \right] \\
&+ \sum_{j=1, j\neq l}^{N} \left(\gamma_0^j g_j + \sum_{m=1}^{h} (\gamma_m^j g_{jk}^1 + \delta_m^j g_{jk}^2) \right)
\end{aligned}
\tag{26a}
$$

$$
\begin{aligned}
\left. \frac{\partial T_{1_{ss}}}{\partial \rho_l} \right|_{R_l} = &\sum_{m=1}^{h} \frac{1}{{R_{max}}^m} \left[\alpha_m \sum_{k=0}^{m} (m-k) \binom{m}{k} (-1)^k R_l^{m-k-1} l_{0l}^k \cos[m\theta_{0l} + k(\phi_l - \theta_{0l})] \right. \\
&\left. + \beta_m \sum_{k=0}^{m} (m-k) \binom{m}{k} (-1)^k R_l^{m-k-1} l_{0l}^k \sin[m\theta_{0l} + k(\phi_l - \theta_{0l})] \right] \\
&+ \gamma_0^l \frac{1}{R_l} - \sum_{m=1}^{h} m \left[\gamma_m^l \left(\frac{1}{R_{\min}} \right)^{-m} R_l^{-m-1} \cos(m\phi_l) + \delta_m^l \left(\frac{1}{R_{\min}} \right)^{-m} R_l^{-m-1} \sin(m\phi_l) \right] \\
&+ \sum_{j=1, j\neq l}^{N} \left(\gamma_0^j g_j' + \sum_{m=1}^{h} (\gamma_m^j g_{jk}'^1 + \delta_m^j g_{jk}'^2) \right)
\end{aligned}
\tag{26b}
$$

where

$$g_j = \begin{cases} \ln(l_{jl}) - \sum_{m=1}^{h} \left(\frac{1}{m}\right) \left(\frac{R_l}{l_{jl}}\right)^m \cos[m(\theta_{jl} - \phi_l)] & \text{if } l_{jl} > R_l \\ \ln(R_l) - \sum_{m=1}^{h} \left(\frac{1}{m}\right) \left(\frac{l_{jl}}{R_l}\right)^m \cos[m(\theta_{jl} - \phi_l)] & \text{if } l_{jl} < R_l \end{cases} \tag{27a}$$

$$g^1_{jk} = \begin{cases} \sum_{k=-1}^{h} \binom{m+k}{k+1} R^m_{min} \frac{R_l^{k+1}}{l_{jl}^{k+m+1}} \cos[(k+1)\phi_l - (k+m+1)\theta_{jl}] & \text{if } l_{jl} > R_l \\ \sum_{k=-1}^{h} (-1)^m \binom{m+k}{k+1} R^m_{min} \frac{l_{jl}^{k+1}}{R_l^{k+m+1}} \cos[(k+1)\theta_{jl} - (k+m+1)\phi_0] & \text{if } l_{jl} < R_l \end{cases} \tag{27b}$$

$$g^2_{jk} = \begin{cases} \sum_{k=-1}^{h} \binom{m+k}{k+1} R^m_{min} \frac{R_l^{k+1}}{l_{jl}^{k+m+1}} \sin[(k+1)\phi_l - (k+m+1)\theta_{jl}] & \text{if } l_{jl} > R_l \\ \sum_{k=-1}^{h} (-1)^m \binom{m+k}{k+1} R^m_{min} \frac{l_{jl}^{k+1}}{R_l^{k+m+1}} \sin[(k+1)\theta_{jl} - (k+m+1)\phi_l] & \text{if } l_{jl} < R_l \end{cases} \tag{27c}$$

$$g'_j = \begin{cases} -\sum_{m=1}^{h} \left(\frac{1}{l_{jl}}\right)^m R_l^{m-1} \cos[m(\theta_{jl} - \phi_l)] & \text{if } l_{jl} > R_l \\ \frac{1}{R_l} + \sum_{m=1}^{h} \left(\frac{1}{R_l}\right)^{m+1} l_{jl}^m \cos[m(\theta_{jl} - \phi_l)] & \text{if } l_{jl} < R_l \end{cases} \tag{27d}$$

$$g'^1_{jk} = \begin{cases} \sum_{k=-1}^{h} (k+1) \binom{m+k}{k+1} R^m_{min} \frac{R_l^k}{l_{jl}^{k+m+1}} \cos[(k+1)\phi_l - (k+m+1)\theta_{jl}] & \text{if } l_{jl} > R_l \\ -\sum_{k=-1}^{h} (-1)^m (k+m+1) \binom{m+k}{k+1} R^m_{min} \frac{1}{R_l^{k+m+2}} l_{jl}^{k+1} \cos[(k+1)\theta_{jl} - (k+m+1)\phi_0] & \text{if } l_{jl} < R_l \end{cases} \tag{27e}$$

$$g'^2_{jk} = \begin{cases} \sum_{k=-1}^{h} (k+1) \binom{m+k}{k+1} R^m_{min} \frac{R_l^k}{l_{jl}^{k+m+1}} \sin[(k+1)\phi_l - (k+m+1)\theta_{jl}] & \text{if } l_{jl} > R_l \\ -\sum_{k=-1}^{h} (-1)^m (k+m+1) \binom{m+k}{k+1} R^m_{min} \frac{1}{R_l^{k+m+2}} l_{jl}^{k+1} \sin[(k+1)\theta_{jl} - (k+m+1)\phi_l] & \text{if } l_{jl} < R_l \end{cases} \tag{27f}$$

A linear system of equations, in the form $\mathbf{\Phi}\gamma = \mathbf{F}$, is obtained by the substitution of Eqs. 25-27 into Eq. 8. The right-hand side vector $\mathbf{F}$ is a function of the fluid temperatures into the pipes. The matrix $\mathbf{\Phi}$, of dimension $\dim \mathbf{\Phi} = [(2h+1)(N+2) \times (2h+1)(N+2)]$, is ill-conditioned and requires preconditioning before the system can be solved for γ:

$$\mathbf{\Phi^T \Phi} \gamma = \mathbf{\Phi^T F} \tag{28}$$

2.3. Time-Dependent Fluid Temperatures

The method presented in Sections 2.1 and 2.2 can be adapted to consider time-dependent fluid temperatures. Step-wise variations of fluid temperatures at each pipe k are considered at each time step n, i.e. over $t^{(n-1)} < t \leq t^n$ (where $t^n = t^{(n-1)} + \Delta t$). In this updating scheme, the initial temperatures in Eqs. 7f and 21 are replaced by the temperature at the end of the latest time step:

$$T_1^{(n-1)} = \sum_{m=1}^{\infty} C_m^{(n-1)} X_1(\rho, \phi; \lambda_1^m) e^{-(\lambda_1^m)^2 \alpha_1 \Delta t} + T_{1_{ss}}^{(n-1)} \tag{29a}$$

$$T_2^{(n-1)} = \sum_{m=1}^{\infty} C_m^{(n-1)} X_2(\rho, \phi; \lambda_2^m) e^{-(\lambda_2^m)^2 \alpha_2 \Delta t} + T_{2_{ss}}^{(n-1)} \tag{29b}$$

The Fourier-Bessel coefficients in Eq. 21 become:

$$C_j^n = \frac{\frac{k_b}{\alpha_1} I_{1j}^{(n-1)} + \frac{k_s}{\alpha_2} I_{2j}^{(n-1)}}{\frac{k_b}{\alpha_1} \int_{\Omega_1} X_1(\rho,\phi;\lambda_1^j)\bar{X}_1(\rho,\phi;\lambda_1^j)d\Omega_1 + \frac{k_s}{\alpha_2} \int_{\Omega_2} X_2(\rho,\phi;\lambda_2^j)\bar{X}_2(\rho,\phi;\lambda_2^j)d\Omega_2} \tag{30}$$

where

$$\begin{aligned}
I_{1j}^{(n-1)} &= \int_{\Omega_1} (T_1^{(n-1)} - T_{1_{ss}}^n)\bar{X}_1(\rho,\phi;\lambda_1^j)d\Omega_1 \\
&= \int_{\Omega_1} (C_j^{(n-1)} X_1(\rho,\phi;\lambda_1^j)e^{-(\lambda_1^j)^2\alpha_1\Delta t} + T_{1_{ss}}^{(n-1)} - T_{1_{ss}}^n)\bar{X}_1(\rho,\phi;\lambda_1^j)d\Omega_1 \\
I_{2j}^{(n-1)} &= \int_{\Omega_2} (T_2^{(n-1)} - T_{2_{ss}}^n)\bar{X}_2(\rho,\phi;\lambda_2^j)d\Omega_2 \\
&= \int_{\Omega_2} (C_j^{(n-1)} X_2(\rho,\phi;\lambda_2^j)e^{-(\lambda_2^j)^2\alpha_2\Delta t} + T_{2_{ss}}^{(n-1)} - T_{2_{ss}}^n)\bar{X}_2(\rho,\phi;\lambda_2^j)d\Omega_2
\end{aligned} \tag{31}$$

where $T_{i_{ss}}^n$ is the solution of the steady-state problem considering the fluid temperatures at the n-th time step, and $T_1^0 = T_2^0 = T^0$.

Eqs. 30 and 31 allow the calculation of the temperature field when fluid temperatures are variable over time and known. In a simulation of a GHE, fluid temperatures are typically unknown. It is however possible to build a system of equation to consider other known values. As an example, assuming the total heat transfer rate, $\dot{q}^n (= \dot{q}'^n H)$, into a GHE containing two pipes is known and that $T_{f_1}^n$ and $T_{f_2}^n$ are equal to the inlet and outlet fluid temperatures:

$$\dot{q}_k'^n = \frac{1}{E_k}\left(T_{f_k}^n - \bar{T}_1^n|_{R_k}\right) \tag{32a}$$

$$\dot{q}'^n = \sum_{k=1}^{N} \dot{q}_k^n \tag{32b}$$

$$\dot{q}'^n H = \dot{m}^n c_p (T_{f_1}^n - T_{f_2}^n) \tag{32c}$$

where $\dot{q}_k'^n$ is the heat transfer rate per unit length from pipe k, $T_{f_k}^n$ is the fluid temperature in pipe k, $\bar{T}_1^n|_{R_k}$ is the average temperature at the outer wall at pipe k, $\dot{m}^n$ is the fluid mass flow rate into the pipes, c_p is the fluid specific heat capacity, and H is the GHE length.

The coefficient updating scheme can also be adapted to consider the fluid temperature variations along the pipes by discretizing the GHE into segments and taking into account the advection of the fluid into the pipes, as commonly done in resistance-capacitance models (Bauer et al. , 2011b; De Carli et al., 2010; Pasquier & Marcotte, 2014; Zarella et al., 2011). This will be addressed in future work.

3. Validation

The proposed method is implemented into Python, using numpy's implementation of the SVD algorithm (Van Der Walt et al. , 2011) and scipy's implementation of Bessel and Hankel functions (Virtanen et al. , 2020) which includes the asymptotic

expansions for large values of the argument. Integrals are evaluated by a quadrature domain technique (Crowdy, 2005).

The accuracy of the proposed method is dependent upon the number of terms considered in the Fourier-Bessel expansion for T_{i_h} (Eq. 20), the number of terms M in the multipole expansion for X_i (Eqs. 15-16), and the number of terms h in the multipole expansion for $T_{i_{ss}}$ (Eqs. 22-23). The number of terms considered in the Fourier-Bessel expansion was fixed at 100 eigenvalues. The solution for X_i is still dependent on the eigenvalues of the Helmholtz equation (Eq. 11) and thus their correct evaluation needs to be validated. The validation of the proposed approach is conducted in three steps. First, the eigenvalues are computed for the geometries presented by Chen et al. (2001, 2004). Second, the steady-state temperature field calculated with the proposed method is compared with the one calculated using the multipole method, as presented by Claesson & Hellström (2011). Finally, the solution of the transient heat conduction is validated against Finite Element Analysis (FEA) simulations for constant and time-dependent fluid temperatures.

3.1. Eigenvalues of the Helmholtz Equation

The calculation of eigenvalues is validated by comparing the results from the presented method to the results of Chen et al. (2001, 2004) for two geometries, calculated from a Boundary Element Method (BEM). The first geometry consists in a single pipe of radius $R_1 = 0.5\ m$ centered into a circular domain of outer radius $R_0 = 2\ m$, as shown on Figure 3. The second geometry consists in two pipes of radius $R_1 = R_2 = 0.3\ m$ symmetrically positioned at a distance $e = 0.5\ m$ from the center of a circular domain of outer radius $R_0 = 1\ m$, as shown on Figure 4. For both geometries, Dirichlet boundary conditions ($X = 0$) are imposed at all domain boundaries ($\partial\Omega_1$, $\partial\Omega_2$ and $\partial\Omega_0$). At this stage, $M = 5$ terms are used in the multipole expansion for X. The proposed method was modified to accommodate Dirichlet boundary conditions on the grout domain Ω_1 (thereby excluding the soil domain Ω_2), which differ from the convection (Eq. 11b) and continuity (Eqs. 11c-11d) boundary conditions presented herein. This change is necessary for comparison with the results of Chen et al. (2001, 2004).

The eigenvalues are extracted using SVD by locating the minimums, corresponding to the eigenvalues λ, of the minimum singular value of $\mathbf{\Phi}$. The extracted eigenvalues are visualized alongside the geometries in Figures 3 and 4. The four former eigenmodes (i.e. the function X), corresponding to the first four non-repeated eigenvalues, are shown in Figures 5 and 6. Table 1 compares the eigenvalues obtained with the proposed method with the eigenvalues obtained by Chen et al. (2001, 2004) using BEM. As shown, the computed eigenvalues are in close agreement with the reference.

Table 1. Comparison of the eigenvalues from the proposed method and Chen et al. (2001, 2004)

Single pipe (Figure 3)		Two pipes (Figure 4)	
BEM in Chen et al. (2001)	Multipole Expansion	BEM in Chen et al. (2004)	Multipole Expansion
$\lambda_1 = 2.06$	$\lambda_1 = 2.05$	$\lambda_1 = 4.50$	$\lambda_1 = 4.50$
$\lambda_2 = 2.23$	$\lambda_2 = 2.22$	$\lambda_2 = 4.50$	$\lambda_2 = 4.56$
$\lambda_3 = 2.67$	$\lambda_3 = 2.66$	$\lambda_3 = 6.37$	$\lambda_3 = 6.40$
$\lambda_4 = 3.22$	$\lambda_4 = 3.21$	$\lambda_4 = 7.16$	$\lambda_4 = 7.11$

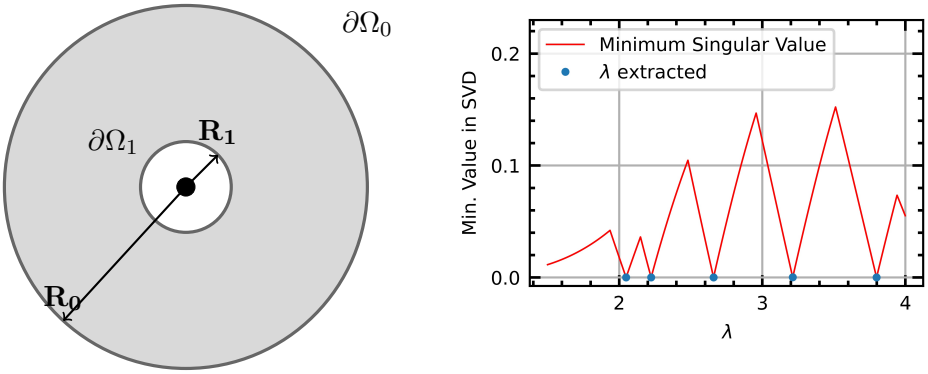

Figure 3. One pipe geometry (Left). Eigenvalues extracted by SVD (Right)

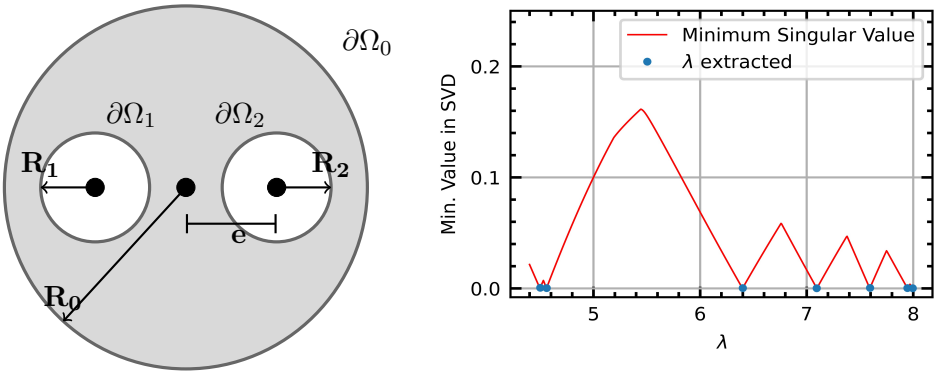

Figure 4. Two pipes geometry (Left). Eigenvalues extracted by SVD (Right)

3.2. Steady-State Temperature Field

The steady-state temperature field is validated by comparing the solution of the steady-state heat equation with non-homogeneous boundary conditions presented in Section 2.2 to the multipole method of Claesson & Hellström (2011) for two asymmetrically positioned pipes, as shown on Figure 7. The dimensions and physical properties associated with the geometry are:

$$\begin{gathered} k_b = 1.5\ W/(m \cdot K), k_s = 2.5\ W/(m \cdot K), R_0 = 0.07\ m \\ O_1 = (-0.03\ m, 0.02\ m), O_2 = (0.03\ m, 0\ m), R_1 = 0.02\ m \\ R_2 = 0.02\ m, \beta_1 = \beta_2 = 1.2, T_{f1} = T_{f2} = 1\ K \end{gathered} \tag{33}$$

The values of $T_{f1} = T_{f2} = 1\ K$ correspond to a unit $(1\ K)$ temperature difference between the fluid and borehole wall temperatures, as considered in Claesson & Hellström (2011). The boundary conditions presented by Claesson & Hellström (2011) are slightly different from the ones considered in Eq. 8. In Claesson & Hellström (2011), the average borehole wall temperature is imposed on $\partial\Omega_0$:

$$\bar{T}_{2_{ss}}\big|_{R_0} = \frac{1}{2\pi}\int_{-\pi}^{\pi} T_{2_{ss}}(R_0, \phi)d\phi = \alpha_0' + \gamma_0' \ln R_0 = 0 \tag{34}$$

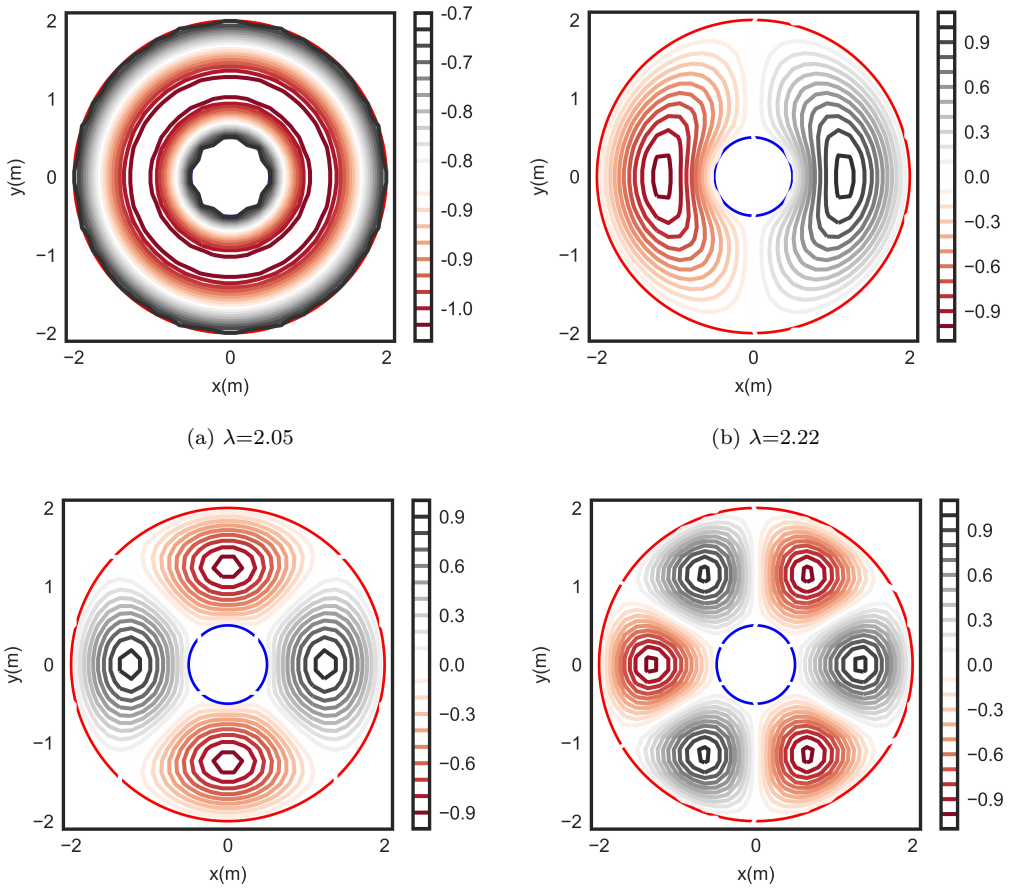

(a) λ=2.05 (b) λ=2.22

(c) λ=2.66 (d) λ=3.21

Figure 5. Eigenmodes of the multipole expansion for one pipe

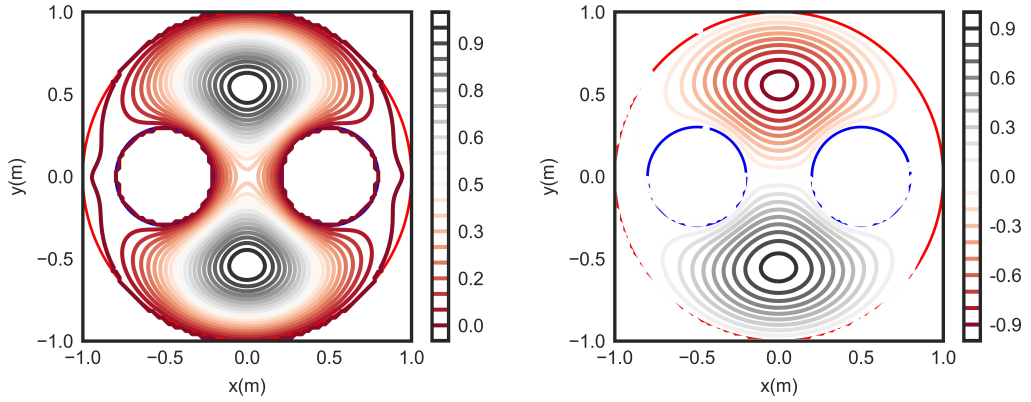

(a) λ=4.50 (b) λ=4.56

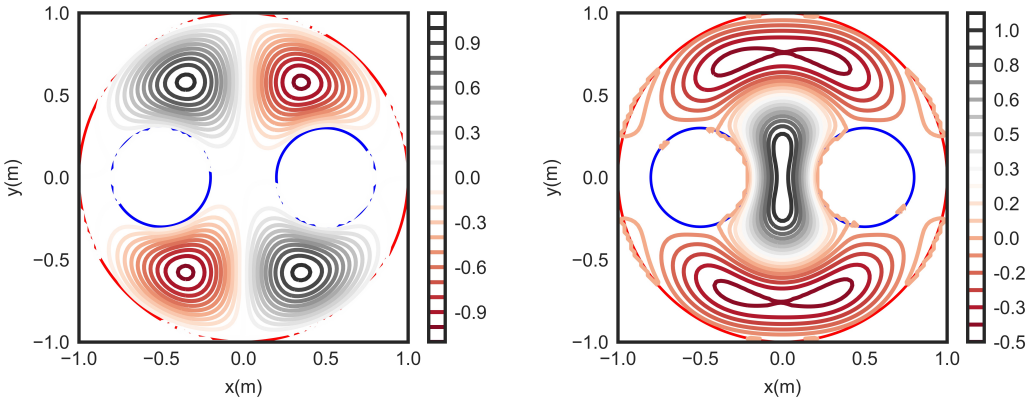

(c) λ=6.40 (d) λ=7.11

Figure 6. Eigenmodes of the multipole expansion for two pipes

where $\bar{T}_{2_{ss}}\big|_{R_k}$ is the perimeter average temperature at a radius R_k and $\bar{T}_{2_{ss}}\big|_{R_0}$ corresponds to the borehole wall temperature.

With this boundary condition, Eq. 23 for the temperature in Ω_2 is modified as follows:

$$T_{2_{ss}} = \bar{T}_{2_{ss}}\big|_{R_0} + \gamma'_0 \ln\frac{\rho_0}{R_0} + \sum_{m=1}^{h}\left[\gamma'_m\left(\frac{\rho_0}{R_{\min}}\right)^{-m}\cos(m\phi_0) + \delta'_m\left(\frac{\rho_0}{R_{\min}}\right)^{-m}\sin(m\phi_0)\right] \tag{35}$$

The method presented in Section 2.2 is still consistent as a solution to the Laplace equations (Eqs. 8 and 34) and can thus be applied with the new boundary condition. Figure 8 shows the steady-state temperature field (left) and a comparison of the temperature profile at $y = 0$ between the proposed method and (Claesson & Hellström, 2011). $h = 15$ terms are used in the multipole expansions for $T_{i_{ss}}$.

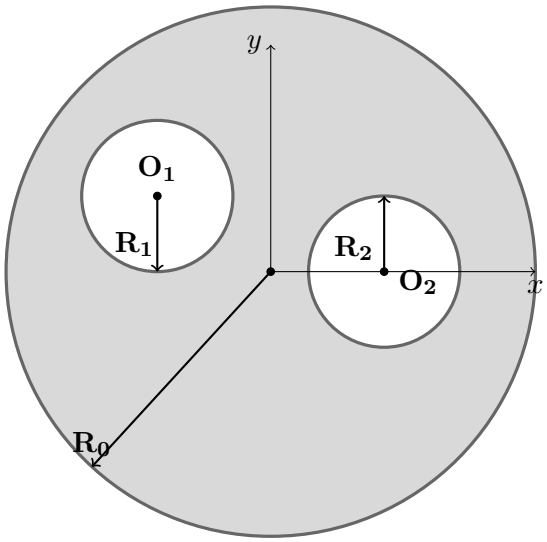

Figure 7. Two asymmetrically positioned pipes geometry

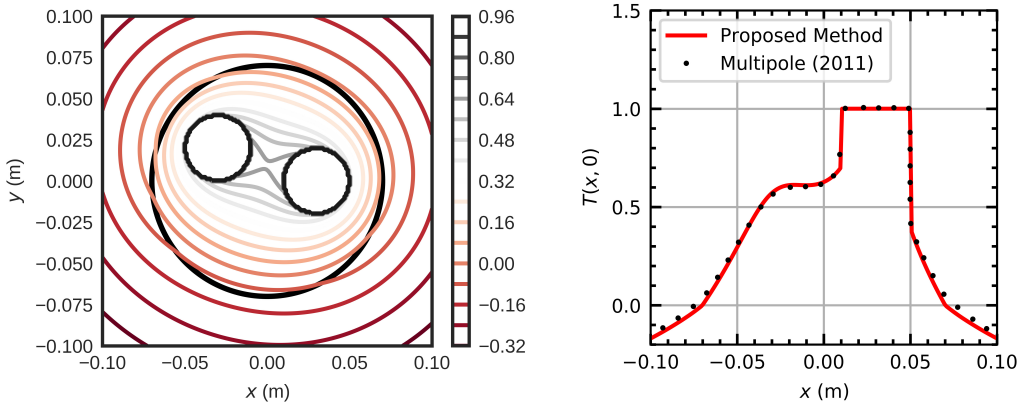

(a) Steady-State Temperature Field

(b) Temperature Profile at $T(x, 0)$

Figure 8. Validation against the multipole method of Claesson and Hellström

3.3. Transient Multipole Expansion

The complete proposed transient multipole expansion method is validated against FEA simulations for two geometries, a single centered pipe (shown on Figure 9) and two symmetrically positioned pipes (shown on Figure 10). FEA simulations are posed with meshes of 10228 nodes and 20216 triangular elements for the single pipe geometry, and 11572 nodes and 22850 triangular elements for the two pipes geometry with an external boundary of $R_e = 100\ m$. For both simulations, 2nd order Lagrange polynomials are used to solve the weak formulation. Backward Euler difference for time derivative is used with a time step $\Delta t = 100$ s.

The dimensions and physical properties of the single pipe geometry are:

$$\begin{gathered} k_b = 0.73\ W/(m \cdot K), k_s = 2.82\ W/(m \cdot K), \alpha_1 = 1.921 \times 10^{-7}\ m^2/s, \\ \alpha_2 = 1.410 \times 10^{-6}\ m^2/s, R_1 = 0.035\ m, R_0 = 0.063\ m, \\ \beta_1 = 0.1985, T^0 = 293.15\ K, T_{f1} = 295.15\ K \end{gathered} \tag{36}$$

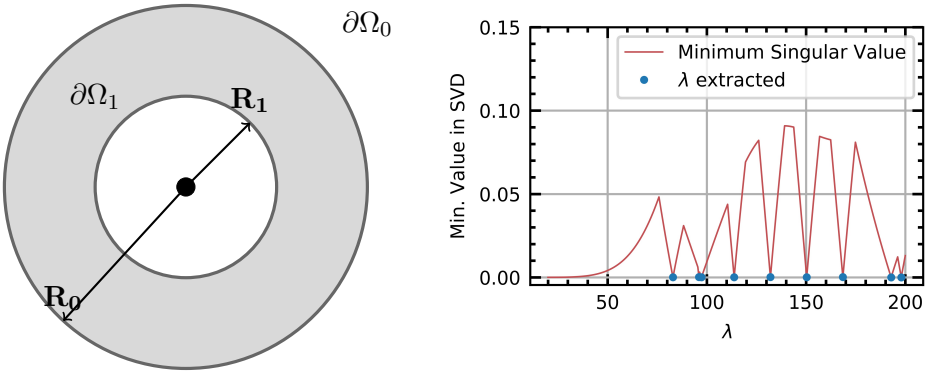

Figure 9. One pipe geometry (Left). Eigenvalues extracted by SVD (Right)

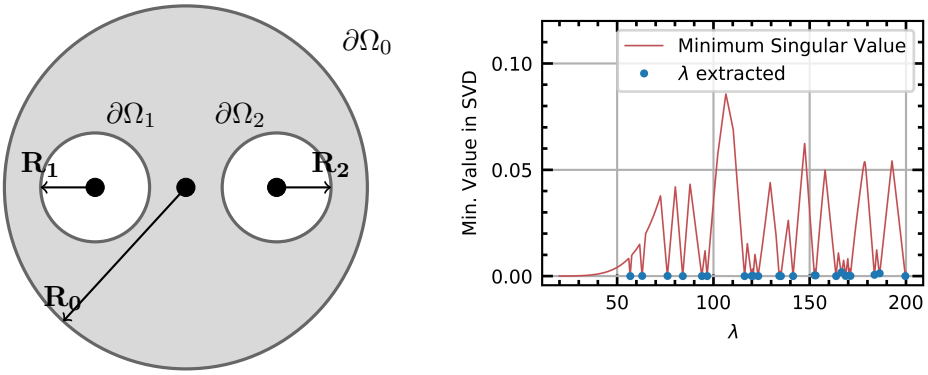

Figure 10. Two pipes geometry (Left). Eigenvalues extracted by SVD (Right)

The dimensions and physical properties of the two pipes geometry are:

$$k_b = 0.73\ W/(m\cdot K), k_s = 2.82\ W/(m\cdot K), \alpha_1 = 1.921\times 10^{-7}\ m^2/s, \alpha_2 = 1.410\times 10^{-6}\ m^2/s$$
$$O_1 = (-0.03\ m, 0), O_2 = (0.03\ m, 0), R_0 = 0.063\ m, R_1 = 0.0167\ m$$
$$T^0 = 293.15\ K, \beta_1 = \beta_2 = 0.4022, T_{f1} = T_{f2} = 295.15\ K \tag{37}$$

Figure 11 presents the total heat transfer rate at the pipe and the average borehole wall temperature for the single pipe geometry and their dependence on the number of terms in the multipole expansions (M and h). Figure 12 presents the same for the two pipes geometry. As shown in both figures, proper values for the parameters M and h are required to ensure convergence of the temperatures and heat transfer rates. For the single pipe geometry, $M = 5$ and $h = 15$ are sufficient to attain convergence, while $M = 7$ and $h = 15$ are needed in the two pipes geometry. The parameter M influences the early transient phase of the temperature and heat transfer rates, and h has a stronger impact on the later stages of the simulation. While the heat transfer rates show good agreement with the FEA simulation, borehole wall temperatures present some differences at early times.

Figures 13 and 14 show the temperature fields calculated from the FEA simulation and the temperature profiles at $y = 0$ calculated from the FEA simulation and the

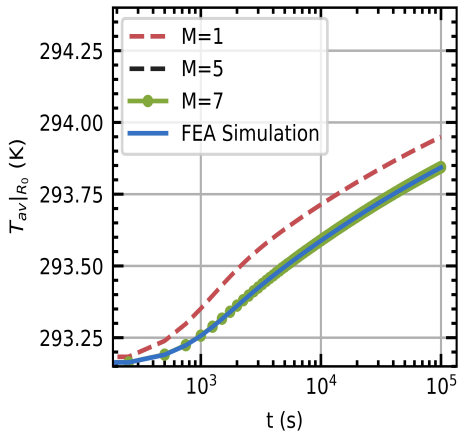

(a) Avg. Borehole Wall Temp. ($h = 15$)

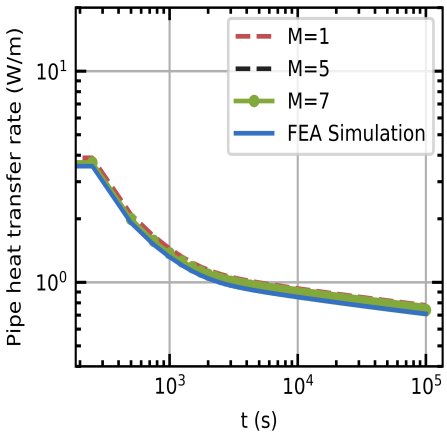

(b) Heat Flow Rate ($h = 15$)

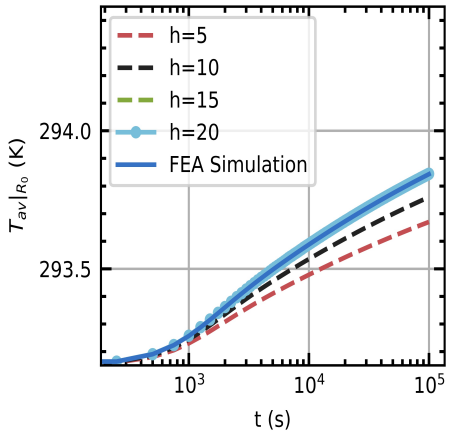

(c) Avg. Borehole Wall Temp. ($M = 5$)

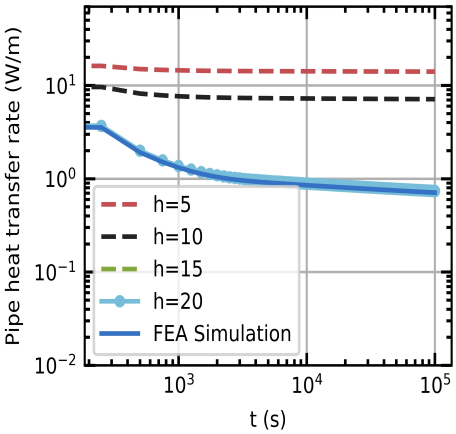

(d) Heat Flow Rate ($M = 5$)

Figure 11. Borehole wall temperature and pipe heat transfer rate (one pipe geometry)

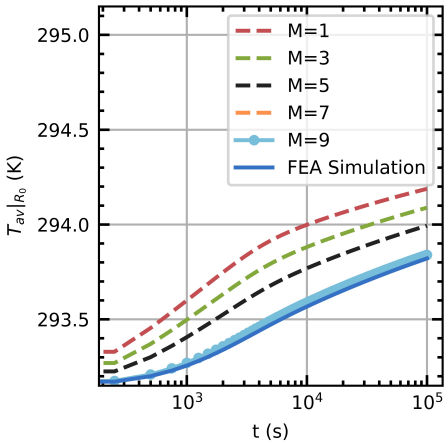

(a) Avg. Borehole Wall Temp. ($h = 15$)

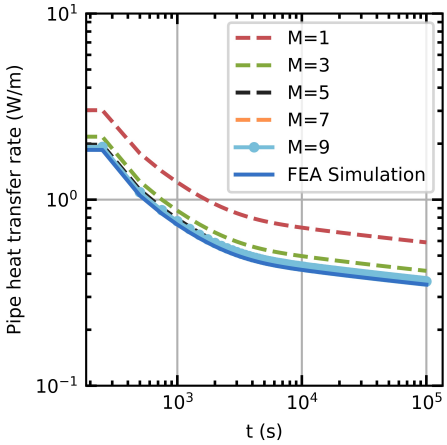

(b) Heat Flow Rate ($h = 15$)

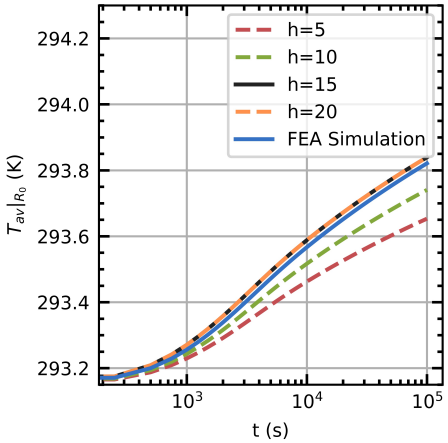

(c) Avg. Borehole Wall Temp. ($M = 7$)

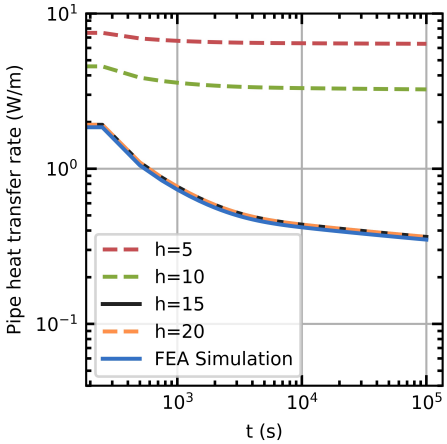

(d) Heat Flow Rate ($M = 7$)

Figure 12. Borehole wall temperature and pipe heat transfer rate (two pipes geometry)

proposed method. The temperature fields and temperatures profile are shown at times $t = 1000$, 10000 and 100000 seconds for both of the single pipe and the two pipes geometries. The same temperature differences are observed as were seen in Figures 11 and 12 for the average borehole wall temperatures.

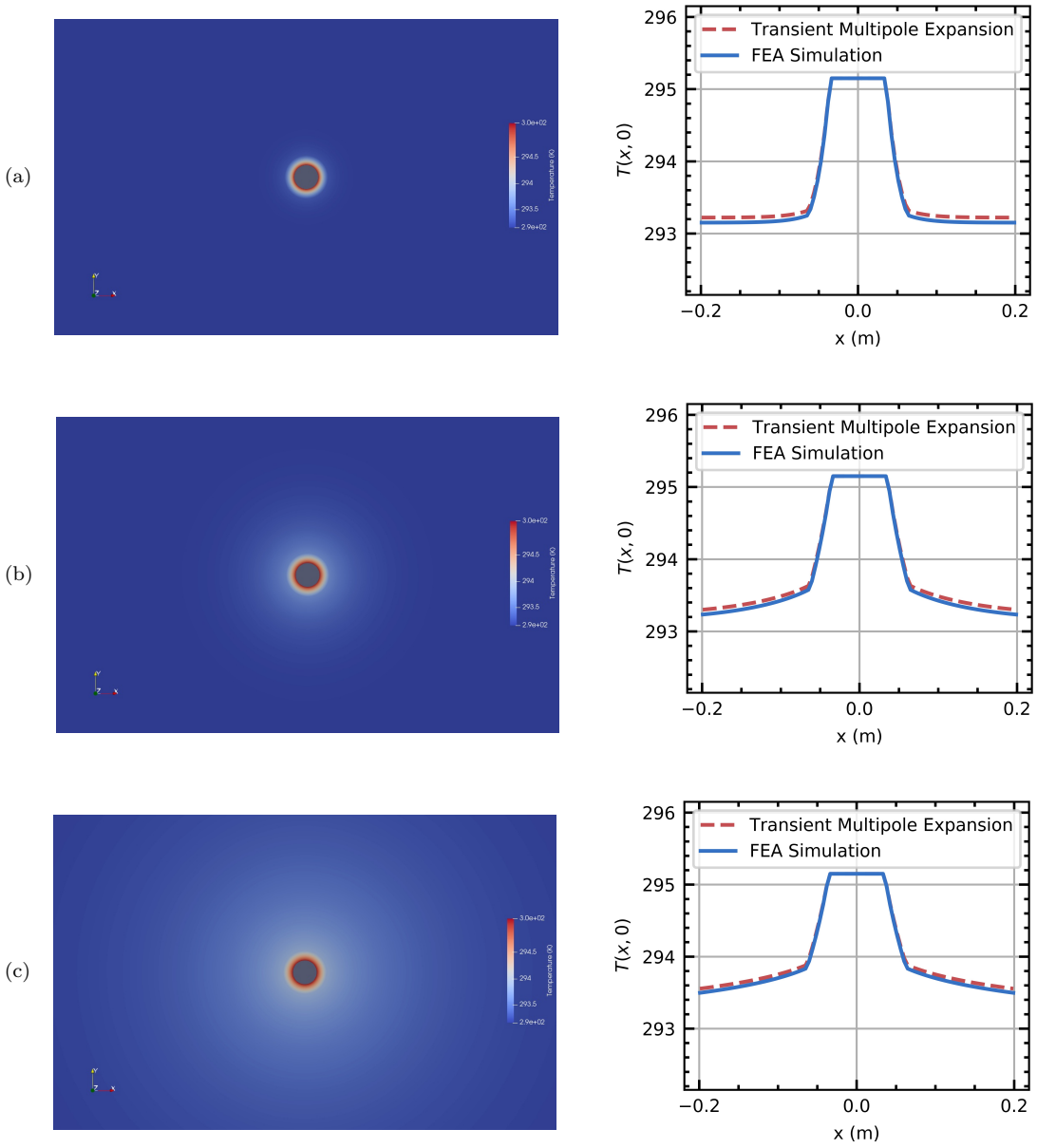

Figure 13. FEA simulation (left) and temperature profile at $y = 0$ (right) for the one pipe geometry: (a) $t = 1000$ s, (b) $t = 10000$ s, and (c) $t = 100000$ s

Finally, the coefficient updating scheme presented in Section 2.3 is used to calculate the fluid temperature variations in the two pipes geometry of Eq. 37. A constant total heat transfer rate per unit length $\dot{q}' = 58\ W/m$ and a constant temperature difference between the pipes $\Delta T = T_{f_1} - T_{f_2} = 1.3\ K$ (representative of a constant fluid mass flow rate) are applied with an initial temperature $T^0 = 293.15\ K$. The simulation time step is $\Delta t = 20\ s$ and the maximum simulation time is $t = 3100\ min$, totaling 9300

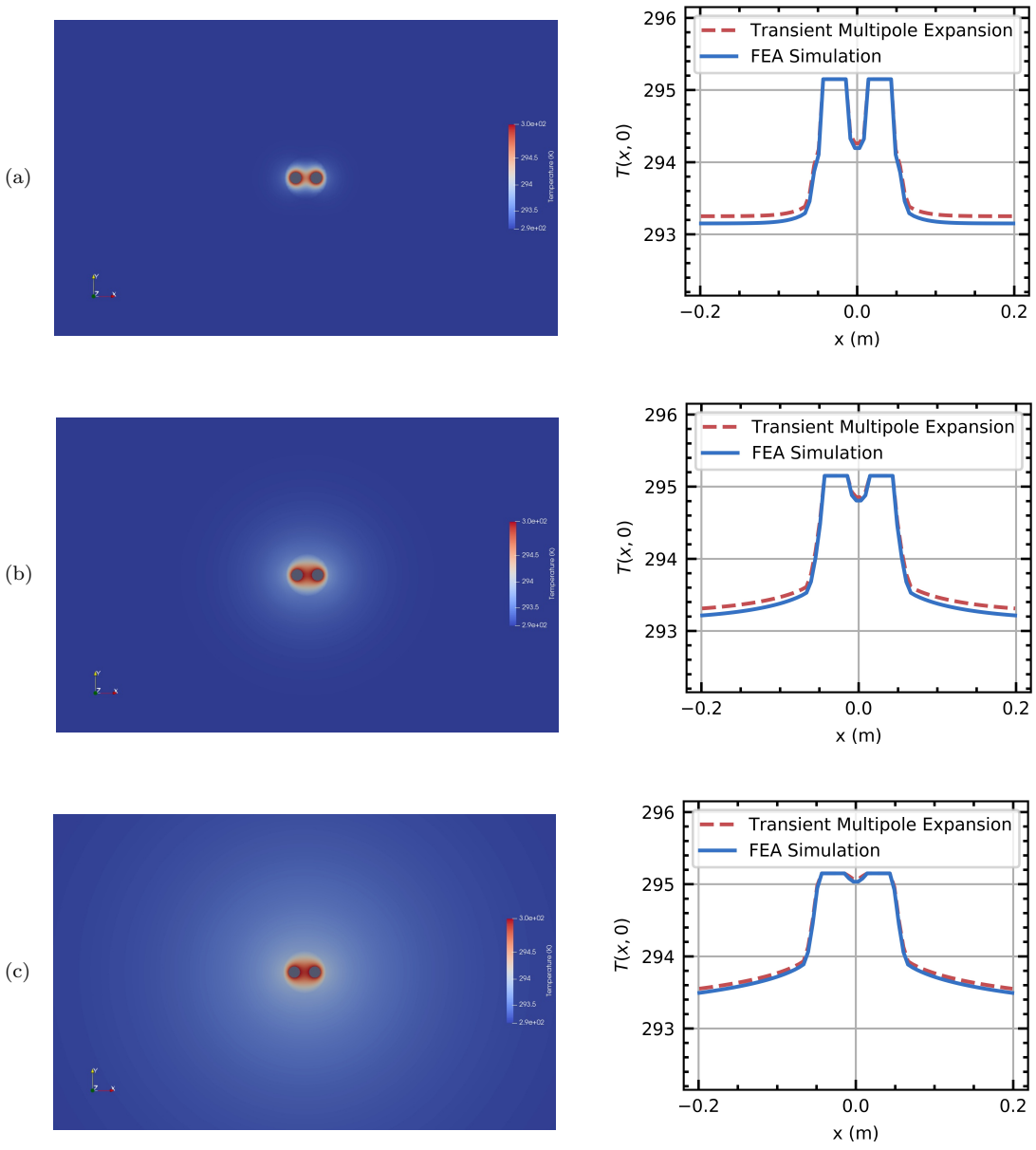

Figure 14. FEA simulation (left) and temperature profile at $y = 0$ (right) for the two pipes geometry: (a) $t = 1000$ s, (b) $t = 10000$ s, and (c) $t = 100000$ s

time steps. FEA calculations take 220 seconds to complete and the presented method takes 80 seconds to complete, including 61 seconds to evaluate the eigenvalues and integrals and 19 seconds to simulate the heat transfer process over all 9300 time steps.

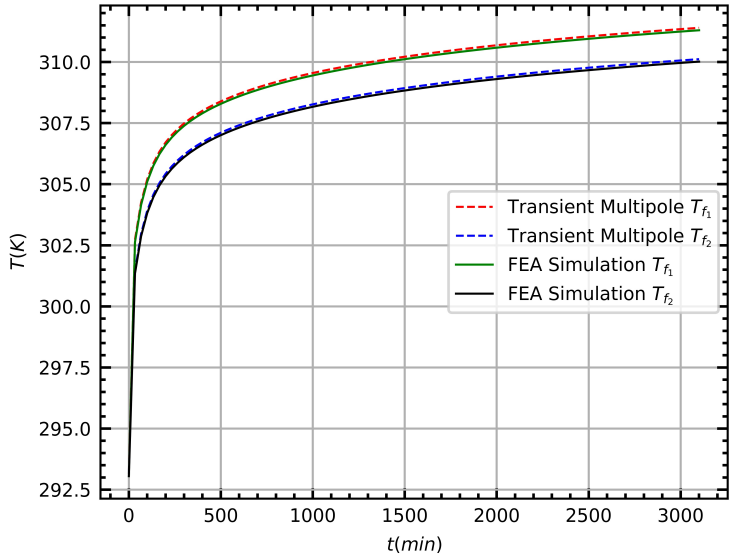

Figure 15. Inlet and outlet fluid temperature variations

4. Conclusion

This paper introduces a new transient multipole method to solve the short-term heat transfer in ground heat exchangers. The method does not require any simplification of the borehole geometry or discretization of the borehole thermal capacitance and can accommodate any number of arbitrarily positioned pipes within the borehole, as opposed to equivalent pipe methods and resistance-capacitance methods found in the literature. The method shows good agreement with reference FEA simulations when considering the 100 former eigenvalues of the expansion, identified from singular value decomposition. The method is then only dependent on the number of terms in the expansions, h and M, without any requirement for mesh generation of the calculation domain. For the considered cases $h = 15$ is sufficient for the steady-state expansion, and $M = 5$ and $M = 7$ are sufficient for the transient expansion in the one pipe and two pipes geometries, respectively. While boundary conditions of imposed fluid temperatures and undisturbed ground temperature as far field are considered in the paper with a unbounded domain, the proposed method can be applied to other types of boundary conditions, as shown in Sections 3.1 and 3.2 for validation against the literature. A coefficient updating scheme is adopted to consider time-dependent fluid temperature. Fluid temperatures can be calculated by updating Fourier-Bessel coefficients and change the boundary conditions at each time step. Further investigation is required to consider the fluid temperature variation along pipes, coupling the proposed method to an advection-convective model of the fluid inside the pipes. The number of considered eigenvalues and the coefficient updating scheme will then be analyzed for their impact on the accuracy and computational efficiency of GCHP simulations.

References

Abdul Azeez, M. F., and A. F. Vakakis. 2000. Axisymmetric transient solutions of the heat diffusion problem in layered composite media. *International Journal of Heat and Mass Transfer* 43 (20):3883–3895.

Abramowitz, M., and I. A Stegun. (1972) Handbook of mathematical functions with formulas, graphs, and mathematical tables *Dept. of Commerce, National Bureau of Standards.*

Bandyopadhyay, G., W. Gosnold and M. Mann. 2008. Analytical and semi-analytical solutions for short-time transient response of ground heat exchangers. *Energy and Buildings* 40 (10):1816–1824.

Bauer, D., W. Heidemann, H. Müller-Steinhagen and H.-J. Diersch. 2011. Thermal resistance and capacity models for borehole heat exchangers. *International Journal of Energy Research* 35 (4):312–320.

Bauer, D., W. Heidemann and H.-J. Diersch. 2011. Transient 3D analysis of borehole heat exchanger modeling. *Geothermics* 40 (4):250–260

Bernier, M., and A. Salim Shirazi 2013. Thermal capacity effects in borehole ground heat exchangers. *Energy and Buildings*, 67:352–364.

Bennet, J., J. Claesson and G. Hellström. 1987. Multipole method to compute the conductive heat flows to and between pipes in a composite cylinder. *Notes on Heat Transfer*. Dept. of Building Physics, Lund University, Lund, Sweden.

Bird, M. D. and C. R. Steele 1992. A solution procedure for Laplace's equation on multiply connected circular domains. *ASME. Journal of Applied Mechanics* 59 (2):398–404.

Bose, J. E., J. Parker and C. Faye. 1985. Design/data manual for closed-loop ground-coupled heat pump systems. *Atlanta, GA: American Society of Heating, Refrigerating, and Air-Conditioning Engineers*.

Brussieux, Y., and M. Bernier 2019. Universal short-time g*-functions: Generation and application. *Science and Technology for the Built Environment* 25 (8):993–1006

De Carli, M., M. Tonon, A. Zarella, and R. Zecchin. 2010. A computational capacity resistance (CaRM) for vertical ground-coupled heat exchangers. *Renewable Energy* 35 (7):1537–1550.

Carslaw, H. S. and J. C. Jaeger. 1959. *Conduction of heat in solids.* (Oxford University Press.) Oxford.

Chen, J. T., J. H. Lin, S. R. Kuo and S. W. Chyuan. 2001. Boundary element analysis for the Helmholtz eigenvalue problems with a multiply connected domain. *Proceedings of Royal Society London A.* 457:2521–2546

Chen, J. T., L. W. Liu, and S. W. Chyuan. 2004. Acoustic eigenanalysis for multiply-connected problems using dual BEM. *Communications in numerical methods in engineering* 20 (6):419–440.

Chen, J. T., I. L. Chen and Y. T. Lee. 2005. Eigensolutions of multiply connected membranes using the method of fundamental solutions. *Engineering Analysis with Boundary Elements* 29 (2):166–174

Chen, J. T., S.-K. Kao, W.-M. Lee and Y. Lee. 2010. Eigensolutions of the Helmholtz equation for a multiply connected domain with circular boundaries using the multipole Trefftz method. *Engineering Analysis With Boundary Elements* 34 (5):463–470

Claesson, J., and J. Bennet. 1987. Multipole method to compute the conductive heat flows to and between pipes in a cylinder. *Notes on Heat Transfer*. Dept. of Building Physics, Lund University, Lund, Sweden.

Claesson, J. and G. Hellström. 2011. Multipole method to calculate borehole thermal resistances in a boreholes heat exchanger. *HVAC& R Research* 17 (6):895–911

Crowdy, D. 2005. Quadrature Domains and Fluid Dynamics. In: Quadrature Domains and Their Applications *Operator Theory: Advances and Applications.* Birkhäuser Basel

Eskilson, P. 1987. *Thermal analysis of heat extraction boreholes*. PhD thesis. Dept. of Building Physics, Lund University, Lund, Sweden.

Graf, J. H. 1893. Ueber die addition und subtraction der argumente bei Bessel'schen functionen nebst einer anwendung *Mathematische Annalen* 43:136–44

Gu, Y. and D. L. O'Neal. 1995. Analytical solution to transient heat conduction in a composite region with a cylindrical heat source. *Journal of Solar Energy Engineering, Transactions of the ASME* 117 (3):242–248.

Gu, Y., and D. L. O'Neal. 1998. Development of an equivalent diameter expression for vertical U-Tubes used in ground-coupled heat pumps *ASHRAE Transactions* 104 (2):347–355.

Haji-Sheikh, A., and J. V. Beck. 2002. Temperature solution in multi-dimensional multi-layer bodies. *International Journal of Heat and Mass Transfer* 45 (9):1865–1877.

Javed, S., and J. Claesson. 2011. New analytical and numerical solutions for the short-term analysis of vertical ground heat exchangers. *ASHRAE Transactions* 117 (1):3-12.

Kita, E., and N. Kamiya. 1995. Trefftz method: an overview. *Advances in Engineering Software* 24 (1-3):3–12.

Lamarche, L. and B. Beauchamp 2007. New solutions for the short-time analysis of geothermal vertical boreholes. *International Journal of Heat and Mass Transfer* 50 (7-8):1408–1419.

Lamarche, L. 2015. Short-time analysis of vertical boreholes, new analytic solutions and choice of equivalent radius *International Journal of Heat and Mass Transfer* 91:800-807.

Li, M., and A. C. K. Lai. 2013. Analytical model for short-time responses of ground heat exchangers with U-shaped tubes: Model development and validation *Applied Energy* 104:510–516.

Linton, C. M., and D. V. Evans. 1990. The interaction of waves with arrays of vertical circular cylinders. *Journal of Fluid Mechanics* 215:549–69.

Liu, C. S. 2008. A highly accurate collocation Trefftz method for solving the Laplace equation in the doubly connected domains. *Numerical Methods for Partial Differential Equations: An International Journal* 24 (1):179–192.

Martin, P. A. 2006. Multiple scattering interaction of time-harmonic wave with N obstacles. *The Journal of the Acoustical Society of America* 121 (5):2473–2474

Mikhailov, M. D. and M. N. Özisik. 1986. Transient conduction in a three-dimensional composite slab. *International Journal of Heat and Mass Transfer* 29 :(2):340–342.

Milošević, N. D. and M. Raynaud. 2004. Analytical solution of transient heat conduction in a two-layer anisotropic cylindrical slab excited superficially by a short laser pulse. *International Journal of Heat and Mass Transfer* 47 (8-9):1627–1641.

Minaei, A., and M. Maerefat. 2017. A new analytical model for short-term borehole heat exchanger based on thermal resistance capacity model. *Energy and Buildings* 146:233–242.

Nguyen, V. P., T. Rabczuk, S. Bordas and M. Duflot. 2008. Meshless methods: a review and computer implementation aspects. *Mathematics and computers in simulation* 79 (3):763–813.

Pasquier, P., and D. Marcotte. 2012. Short-term simulation of ground heat exchanger with an improved TRCM. *Renewable Energy* 46:92–99.

Pasquier, P., and D. Marcotte 2014. Joint use of quasi-3D response model and spectral method to simulate borehole heat exchanger. *Renewable Energy* 51:281–299.

Salt, H. 1983. Transient conduction in a two-dimensional composite slab-I. Theoretical development of temperature modes. *International Journal of Heat and Mass Transfer* 26 (11):1611–1616.

Shonder, J. A., and J. V. Beck. 1999. Determining effective soil formation properties from field data using a parameter estimations technique. *ASHRAE Transactions* 105 (1):458–466.

Stehfest, H. 1970. Remark on algorithm 368: Numerical inversion of Laplace transforms. *Communications of the ACM* 13 (10):624

Strang, G. and G. J. Fix. 1973. *An Analysis of the Finite Element Method.* Prentice-Hall, Englewood Cliffs.

Tittle, C. W. 1965. Boundary value problems in composite media: Quasi-orthogonal functions. *Journal of Applied Physics* 36 (4):1486–1488.

Trefftz, E. 1926. Ein Gegenstück zum Ritzschen Verfahren. *Proceedings of the 2nd International Congress of Applied Mechanics, Zurich.* 131–137.

Van Der Walt, S., S. C. Colbert and G. Varoquaux. 2011. The NumPy Array: A Structure for Efficient Numerical Computation. *Journal of Computing in Science & Engineering* 13

(2):22–30.

Virtanen, P., R. Gomers, T. E. Oliphant, M. Haberland, T. Reddy, D. Cournapeau, E. Burovski, P. Peterson, W. Weckesser, J. Bright, S. J. Van Der Walt, M. Brett, J. Wilson, K. J. Millman, N. Mayorov, A. R. J. Nelson, E. Jones, R. Kern, E. Larson, C. J. Carey, I. Poltat, Y. Feng, E. W. Moore, J. Vanderplas, D. Laxalde, J. Perktold, R. Cimrman, I. Henriksen, E. A. Quintero, C. R. Harris, A. M. Archibald, A. H. Ribeiro, F. Pedregosa and P. Van Mulbregt. 2020. SciPy 1.0: fundamental algorithms for scientific computing in Python. *Journal of Nature Methods* 17 (3):261–272.

Wu, X. H., and A. A. Kishk. 2008. Hybrid of method of moments and cylindrical eigenfunction expansion to study substrate integrated waveguide circuits. *IEEE Transactions on Microwave Theory and Techniques* 56 (10):2270–2276

Xu, X., and J. Spliter. 2006. Modeling of vertical ground loop heat exchangers with variable convective resistance and thermal mass of the fluid. *Proceedings of Ecostock America*: Pomona.

Yang, Y., and M. Li. 2014. Short-time performance of composite-medium line-source model for predicting responses of ground heat exchangers with single U-shaped tube. *International Journal of Thermal Sciences* 82:130–137.

Yavuzturk, C. 1999. *Modelling of vertical ground loop heat exchangers for ground source heat pump systems*. PhD Thesis. Oklahoma State University. Stillwater OK, United States of America.

Young, T. R. 2004. *Development, verification, and design analysis of the borehole fluid thermal mass model for approximating short term borehole thermal response*. M.Sc. Thesis, Oklahoma State University. Stillwater OK, United States of America.

Zarrella, A., M. Scarpa and M. De Carli. 2011. Short time step analysis of vertical ground-coupled heat exchangers: The approach of CaRM. *Renewable Energy* 36 (9):2357–2367.

Záviška, F. 1913. Uber die Beugung elektromagnetischer Wellen an parallelen, unendlich langen Kreiszylindern. *Annalen der Physik* 345 (5):1023–1056